Low- and high-temperature magnetism of Cr and Fe nanoclusters in iron-chromium alloys

Chu-Chun Fu,[1] M. Y. Lavrentiev,[2] R. Soulairol,[1] S. L. Dudarev,[2] and D. Nguyen-Manh[2]
[1]*CEA, DEN, Service de Recherches de Métallurgie Physique, F-91191 Gif-sur-Yvette, France*
[2]*CCFE, Culham Science Centre, Abingdon, Oxfordshire OX14 3DB, United Kingdom*
(Received 24 September 2014; revised manuscript received 12 March 2015; published 27 March 2015)

Low-energy magnetic states and finite-temperature properties of Cr nanoclusters in bulk bcc Fe and Fe nanoclusters in bulk Cr are investigated using density functional theory (DFT) and the Heisenberg-Landau Hamiltonian based magnetic cluster expansion (MCE). We show, by means of noncollinear magnetic DFT calculations, that magnetic frustration caused by competing ferromagnetic and antiferromagnetic interactions either strongly reduces local magnetic moments while keeping collinearity or generates noncollinear magnetic structures. Small Cr clusters generally exhibit collinear ground states. Noncollinear magnetic configurations form in the vicinity of small Fe clusters if antiferromagnetic Fe-Cr coupling dominates over ferromagnetic Fe-Fe interactions. MCE predictions broadly agree with DFT data on the low-energy magnetic structures, and extend the DFT analysis to larger systems. Nonvanishing cluster magnetization caused by the dominance of Fe-Cr over Cr-Cr antiferromagnetic coupling is found in Cr nanoclusters using both DFT and MCE. Temperature dependence of magnetic properties of Cr clusters is strongly influenced by the surrounding iron atoms. A Cr nanocluster remains magnetic until fairly high temperatures, close to the Curie temperature of pure Fe in the large cluster size limit. Cr-Cr magnetic moment correlations are retained at high temperatures due to the coupling of interfacial Cr atoms with the Fe environment. Variation of magnetization of Fe-Cr alloys as a function of temperature and Cr clusters size predicted by MCE is assessed against the available experimental data.

DOI: 10.1103/PhysRevB.91.094430 PACS number(s): 75.50.Bb, 75.75.−c, 64.70.kd, 64.75.Op

I. INTRODUCTION

Alloys of magnetic metals exhibiting ferromagnetic (FM) and antiferromagnetic (AF) ordering tendencies often have complex magnetic properties, bcc Fe-Cr alloys being a representative example of such magnetic materials. Magnetic frustration occurs in regions close to structural defects (surfaces, grain boundaries) and chemical heterogeneities (matrix-precipitate interfaces and small clusters). High-Cr iron alloys are of significant technological interest due to the beneficial effect of Cr on their corrosion and radiation resistance. Fe-Cr alloys-based ferritic steels have recently attracted attention as candidate structural materials for the next generation fission and future fusion reactors [1–3].

The formation of Cr nanoclusters and precipitates in bcc Fe, and Fe nanoclusters in bcc Cr is a well-known phenomenon occurring in Fe-Cr alloys during the so-called $\alpha - \alpha'$ phase decomposition. Such decomposition is observed if the chemical content of the alloy is inside the miscibility gap of the binary Fe-Cr phase diagram. Phase decomposition may also be induced or accelerated by irradiation [4]. Many studies showed a fundamental link between magnetism and various thermodynamic, segregation, defect, and kinetic properties of bulk Fe-Cr alloys [5–13]. In particular, magnetic properties of Fe and Cr nanoclusters and precipitates affect diffusion of vacancies and solutes [14–17] as well as the Curie temperature of the alloys [18,19].

In addition, an investigation of magnetism of nanoclusters also makes it possible to explore how Fe and Cr behave if magnetic frustration occurs. We also aim at comparing magnetic properties of nanoclusters with magnetic characteristics of the respective Fe and Cr pure systems where we know, for example, that magnetism of Cr atoms is more sensitive to their local environment than magnetism of Fe atoms [20]. The effect of magnetic frustration on magnetic ground states of pure or mixed Cr and Mn clusters supported on metal substrates (Fe, Cu, Ag) was explored by means of first-principles [21–23] and tight-binding electronic-structure calculations [24,25]. Magnetic structure of clusters was analyzed using both collinear and noncollinear approximations. Using a noncollinear first-principles approach, Bergman *et al.* predicted the occurrence of noncollinear magnetic configurations if antiferromagnetism of a Cr-Mn cluster on the Cu(111) surface was frustrated [21]. Robles *et al.* [24] showed that the tendency of Cr clusters supported on bcc Fe to form noncollinear magnetic configurations is generally weaker than of those supported on fcc Fe substrates. In the former case, magnetic frustration only occasionally gives rise to noncollinear magnetic configurations. Furthermore, small free-standing Fe-Cr clusters exhibit preference for collinear magnetic ordering even in the presence of magnetic frustration [26]. On the other hand, to the best of our knowledge, no detailed investigation of magnetic Cr nanoclusters in bulk bcc Fe at the first-principles level, taking into account both longitudinal and transverse magnetic degrees of freedom, has ever been performed. Instead, magnetic properties of clusters and precipitates were treated in the collinear approximation [6,14,15,27].

In a recent paper [28], we investigated interfaces of large precipitates in Fe-Cr alloys and showed that magnetic interactions across a planar Fe/Cr interface can result in the noncollinearity of magnetic moments of Cr atoms with respect to the ferromagnetically ordered moments of iron atoms, in agreement with experimental neutron diffraction data [29]. In the following, using the same simulation methodology, we investigate magnetism of Cr clusters in FM bcc Fe, as well as Fe clusters in AF bcc Cr. Simulations were performed using two complementary approaches: density functional theory (DFT) and magnetic cluster expansion (MCE). The use of reduced localized basis sets in DFT calculations makes it possible to perform an extensive and systematic *ab initio* study going

beyond the collinear approximation. At the same time, the recently developed MCE model [30] was parametrized and successfully applied to the study of Fe-Cr alloys, to explore magnetic properties of the alloys in a broad temperature interval [31] as well as to model the variation of the Curie temperature as a function of chemical composition [32]. The broad range of applicability of the MCE model is confirmed by its recent application to fcc Fe-Ni alloys [33]. Magnetic noncollinearity of large Cr clusters found in MCE simulations [19] prompted us to investigate the origin of magnetic order at Fe/Cr interfaces [28]. Good agreement between DFT and MCE results established in that study now makes it possible to combine DFT and MCE approaches in the investigation of noncollinear magnetism of Cr and Fe nanoclusters of various shapes and sizes, carried out below.

In what follows, we explore how the magnetic structure and energy of Cr(Fe) clusters in bcc Fe(Cr) matrix depend on Fe-Fe, Fe-Cr, and Cr-Cr magnetic interactions. In particular, we investigate whether magnetic frustration, resulting from the competing first- and second-nearest-neighbor Fe-Cr antiferromagnetic and first-nearest-neighbor Cr-Cr antiferromagnetic interactions and responsible for the magnetic noncollinearity at planar interfaces [28], also gives rise to magnetic noncollinearity of Cr(Fe) clusters.

Extensive DFT calculations of the lowest-energy collinear and noncollinear magnetic structures of small (dimer, trimer, etc.) and larger nanoclusters, with (100) and/or (110) facets and containing up to 70 solute atoms, were performed to define conditions for the occurrence of noncollinear magnetic configurations. DFT results are also used for validating parameters of the MCE model. MCE simulations can describe fairly large clusters, which are presently beyond the capacity of DFT calculations. We study the evolution of magnetic properties as functions of cluster size, starting from the very small clusters, where interface effects are important, to fairly large precipitates, where magnetic structure becomes similar to that of the bulk material. MCE-based Monte Carlo simulations are then used to investigate finite-temperature magnetic properties, which are compared with the available experimental information.

The paper is organized as follows. In Sec. II, we describe the two computational approaches used in this study. DFT results are given in Sec. III. MCE simulations, including the analysis of high-temperature properties, are summarized in Sec. IV. Conclusions and summary are given in Sec. V.

II. CALCULATION METHODS

A. First-principles approach

First-principles calculations were performed using DFT, as implemented in the SIESTA code [34]. In all the calculations, the alloys are treated as spin polarized, and the treatment of magnetism goes beyond the collinear approximation [35]. Spin-orbit coupling effects are not taken into account. The validity of noncollinear calculations with SIESTA has already been illustrated earlier [28,36]. The Mulliken population analysis was used to evaluate the atomic magnetic moments $\mathbf{M}_i$, i.e., the local magnetic moments associated with each of the atoms. The magnetization of a cluster is defined as the average value of moments of all the atoms in the cluster. All the results presented in this paper were obtained using the generalized gradient approximation (GGA) exchange-correlation functional in the Perdew-Burke-Ernzerhof (PBE) form [37].

Regarding other DFT approximations, the core electrons are replaced by nonlocal norm-conserving pseudopotentials (NCPP), while the valence ($4s$ and $3d$) electrons are described by linear combinations of numerical pseudoatomic orbitals. The pseudopotentials and the basis sets for Cr and Fe are the same as in Refs. [16,20,38], where the accuracy of Cr and Fe pseudopotentials and basis sets was tested against the relevant known energy and magnetic properties. They were shown to agree satisfactorily with both the experimental data and accurate DFT values computed using the projector augmented wave (PAW) atomic data [20].

Supercell calculations were performed to model Cr nanoclusters in bcc ferromagnetic (FM) Fe, and Fe clusters in bcc antiferromagnetic (AF) Cr. Clusters containing from 2 to 35 atoms were modeled using cubic supercells of $4 \times 4 \times 4$ and $5 \times 5 \times 5$ times the lattice parameter of the cubic unit cell (a_0), containing, respectively, 128 and 250 atoms. The largest 41- and 70-atom clusters were studied using a tetragonal $4\sqrt{2} \times 4\sqrt{2} \times 8\ a_0$ cell containing 512 atoms.

Calculations were performed assuming constant pressure conditions, i.e., the structures were optimized by relaxing both atomic positions as well as the shape and volume of the supercell. All the residual force and stress components were verified to be less than 0.04 eV/Å and 5 kbar, respectively.

The k-point grids used in various supercell calculations were adjusted according to the number of atoms in a cell. The grids were chosen to achieve k-space sampling equivalent to a bcc cubic unit cell with a $12 \times 12 \times 12$ shifted k grid. The Methfessel-Paxton broadening scheme with 0.3 eV width was used. The calculated magnetic structures and cluster formation energies were well converged with respect to the choice of k-point grids. A typical error bar for the difference between the total energies of two magnetic states computed for the same cluster is estimated to be 0.03 eV.

We have also calculated the formation energy of a Cr atom in a cluster. For a system comprising N lattice Fe atoms and a cluster of n Cr atoms, this formation energy is defined as

$$E^f/\mathrm{Cr} = \frac{1}{n}[E(n\mathrm{Cr}, N\mathrm{Fe}) - nE(\mathrm{Cr}) - NE(\mathrm{Fe})], \qquad (1)$$

where $E(n\mathrm{Cr}, N\mathrm{Fe})$ is the total energy of a system containing a n-atom Cr cluster, and $E(\mathrm{Cr})$ and $E(\mathrm{Fe})$ are, respectively, the energy per atom in perfect AF bcc-Cr and FM bcc-Fe.

B. Magnetic cluster expansion

A magnetic cluster expansion (MCE) model was proposed and developed in Ref. [30] as an extension of conventional cluster expansion [39]. Cluster expansion was successfully used in an earier study of Fe-Cr alloys [40], where we found that it could only describe chemical order and disorder in the alloy and could not model its magnetic properties. The MCE Heisenberg-Landau–type Hamiltonian was then applied [30] to the treatment of both configurational and magnetic degrees of freedom of the alloy. A similar Hamiltonian was applied to

modeling antiferromagnetic-ferromagnetic phase transitions and related volume changes in Fe-Rh alloys [41].

The energy of an alloy in MCE depends both on discrete lattice site occupation variables σ_i (for example, $\sigma_i = +1$ for Fe, $\sigma_i = -1$ for Cr) and magnetic moments $\mathbf{M}_i$ of atoms occupying the sites. The magnetic moment vectors have variable direction and magnitude. The MCE Hamiltonian is a sum of conventional cluster expansion terms and magnetic terms. The magnetic part of the Hamiltonian has the Heisenberg-Landau form. Magnetic properties of an alloy explicitly depend on its atomic configuration via the site-dependent Landau self-energy terms, which in a self-consistent way determine the magnitudes of all the atomic magnetic moments, and on the intersite Heisenberg magnetic interaction parameters. Atomic configurations and magnetic degrees of freedom are not independent since the magnetic configuration of an alloy depends on its atomic configuration via the Landau self-energy coefficients A_i, B_i and intersite Heisenberg exchange interaction parameters J_{ij} on the type of atoms occupying each lattice site, and the nearest-neighbor environment. The energy of an alloy configuration in MCE depends not only on the occupation of lattice sites by atoms of various types but also on the magnitude and orientation of atomic magnetic moments.

In what follows, we use an MCE parametrization where only two-atom clusters are retained in the magnetic and nonmagnetic parts of the Hamiltonian

$$\begin{aligned}\mathcal{H}(\{\sigma_i\},\{\mathbf{M}_i\}) &= NI^{(0)} + I^{(1)}\sum_i \sigma_i + \sum_{ij} I_{ij}^{(2)}\sigma_i\sigma_j \\ &+ \sum_i \left(A^{(0)} + A^{(1)}\sigma_i + \sigma_i \sum_j A_{ij}^{(2)}\sigma_j\right)\mathbf{M}_i^2 \\ &+ \sum_i \left(B^{(0)} + B^{(1)}\sigma_i + \sigma_i \sum_j B_{ij}^{(2)}\sigma_j\right)\mathbf{M}_i^4 \\ &+ \sum_{ij}\left[J_{ij}^{(0)} + J_{ij}^{(1)}(\sigma_i+\sigma_j) + J_{ij}^{(2)}\sigma_i\sigma_j\right]\mathbf{M}_i\cdot\mathbf{M}_j. \quad (2)\end{aligned}$$

Here, N is the total number of atoms and $I^{(i)}$ are the nonmagnetic cluster expansion coefficients. Summation over i and j involves atoms occupying nearest-neighbor coordination shells. The functional form of Eq. (2) guarantees that the magnetic self-energy terms, and hence the directions and magnitudes of magnetic moments $\mathbf{M}_i$ predicted by the model, depend on the local environment of each atom. Numerical values of parameters of Hamiltonian (2) for Fe-Cr alloys are given in [30]. In the MCE, both first- and second-nearest-neighbor Fe-Cr interaction parameters strongly favor antiferromagnetic alignment of moments. This Hamiltonian allows fast Monte Carlo simulations over a wide range of atomic and magnetic configurations, concentrations, and temperatures.

III. DFT RESULTS AND DISCUSSIONS

A. Cr clusters in FM bcc Fe

We start by investigating Cr nanoclusters in FM bcc Fe. Aside from the very small clusters, we consider clusters having the lowest-energy Fe/Cr interfaces, that is, the (100)- and the (110)-type interfaces found in our previous DFT studies [28]. Four groups of clusters have been examined: (i) small clusters of 2, 3, 4, and 5 Cr atoms, (ii) cubic clusters with (100) facets, containing 9 and 35 Cr atoms, (iii) octahedral clusters with 6, 15, 19, and 24 Cr atoms that have only the (110) facets, and (iv) mixed clusters with both (100) and (110) interfaces containing 13, 14, 16, 18, 22, 41, and 70 Cr atoms. The most relevant configurations of the small clusters are plotted in Fig. 1, and some representative octahedral, cubic, and mixed clusters are shown in Fig. 2. A full description of configurations of cubic, octahedral, and mixed clusters are given in Table I in terms of the number of Cr atoms in successive atomic planes in a (100) direction.

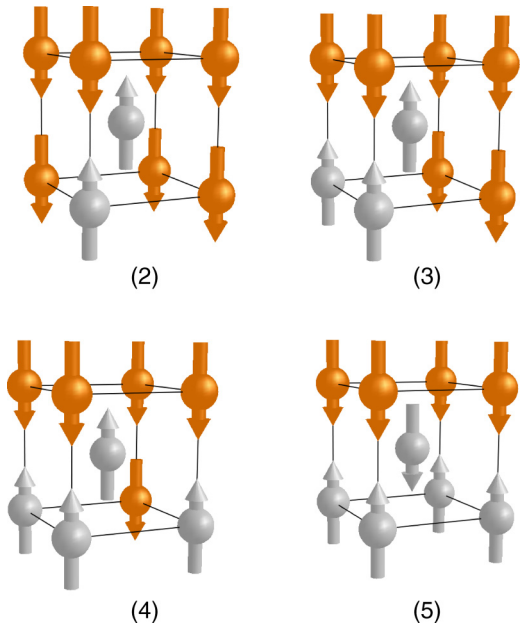

FIG. 1. (Color online) Schematic representation of atomic positions and atomic magnetic moments (arrows) in small Cr clusters containing between 2 and 5 atoms in a bcc Fe lattice. Gray and yellow spheres denote Cr and Fe atoms, respectively. Cubic unit cells are drawn with solid lines.

To investigate the occurrence and stability of collinear (Col) and noncollinear (NCol) magnetic configurations of

TABLE I. Structure of octahedral, cubic, and mixed Cr n-atom clusters defined by the number of Cr atoms in the successive (100) atomic planes.

	Octahedral		
$n = 6$	1-4-1	$n = 19$	1-4-9-4-1
$n = 15$	1-4-5-4-1	$n = 24$	1-4-5-4-5-4-1
	Cubic		
$n = 9$	4-1-4	$n = 35$	9-4-9-4-9
	Mixed		
$n = 13$	4-5-4	$n = 14$	5-4-5
$n = 16$	4-4-4-4	$n = 18$	4-5-4-5
$n = 22$	4-5-4-5-4	$n = 41$	2-7-8-7-8-7-2
$n = 70$	4-12-13-12-13-12-4		

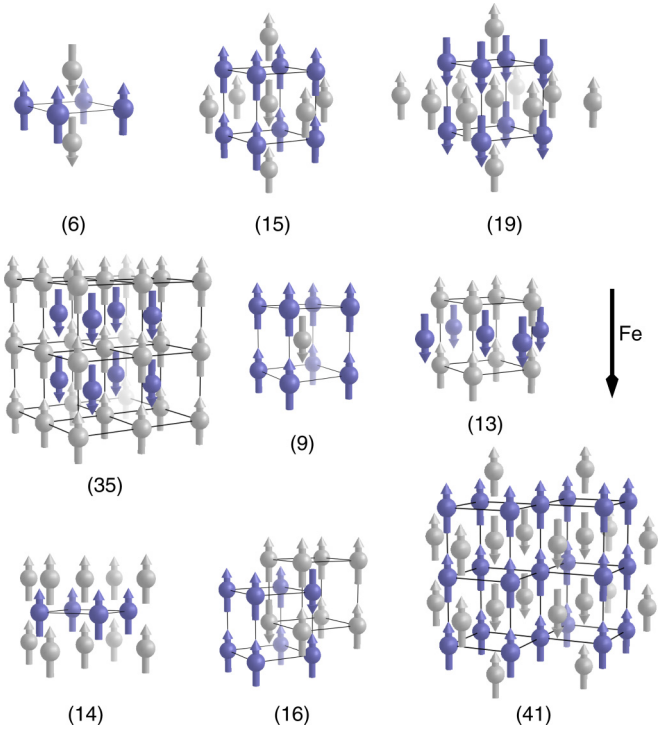

FIG. 2. (Color online) Schematic representations of atomic positions and atomic magnetic moments (arrows) of some representative Cr clusters in the lowest-energy collinear state. Some cubic unit cells are drawn for clarity. The orientation of Fe magnetic moments is also shown.

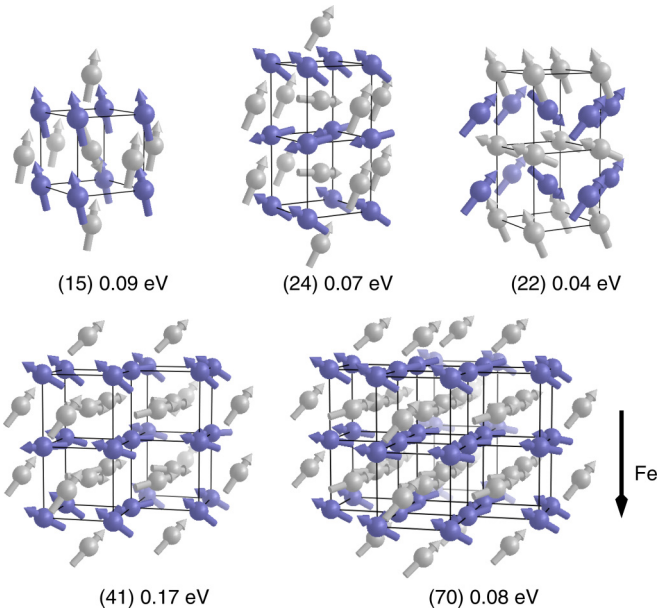

FIG. 3. (Color online) Schematic representations of atomic positions and local magnetic moments (arrows) of Cr clusters containing 15, 24, 22, 41, and 70 atoms in their metastable NCol configurations. The energy difference, per cluster, between these configurations and the respective collinear ground state is shown. Orientation of the lattice Fe moments is also indicated.

a given cluster, we initialized DFT calculations assuming various arrangements of local magnetic moments, in terms of orientations and magnitudes of the moments. As was shown in many previous DFT studies [6,20], an isolated Cr atom in FM-Fe lattice has a large induced magnetic moment, which is antiparallel to the moments of surrounding Fe atoms. Such antiferromagnetic (AF) coupling tendency between Cr and Fe atoms, particularly between the nearest- and next-nearest Fe-Cr neighbors (respectively *nn* and *nnn*), also determines the magnetic configuration of small Cr clusters, where any of the Cr atoms has at most three Cr *nn* (Fig. 1). We have found that the magnetic ground states of all these clusters are collinear (Col), and there are no NCol configurations forming as metastable local minima of energy. Due to competition between AF coupling in Fe-Cr and Cr-Cr *nn* pairs of atoms in these clusters, the magnitude of moments on central Cr atoms decreases with the increasing number of Cr *nn*. This magnitude varies from 2.37 μ_B, 2.05 μ_B, to 0.56 μ_B when the number of Cr *nn* increases from 1 to 3. The particularly small magnitude of the moment on the central atom in a 4-Cr cluster suggests strong magnetic frustration. For the central atom in a 5-Cr cluster with 4 Cr and 4 Fe *nn* (Fig. 1), AF Cr-Cr coupling dominates over Fe-Cr coupling. The local moment on such Cr atom is parallel to the Fe moments, and the magnitude of the moment is small (0.95 μ_B). These results are in agreement with previous DFT calculations [6] performed in the collinear approximation.

For the two cubic clusters comprising 9 and 35 Cr atoms, all the NCol initial configurations are unstable, and decay to a Col arrangement. This result is consistent with our previous findings that infinite planar Fe/Cr (100) interfaces do not promote magnetic noncollinearity [38]. On the other hand, Cr and Fe local moments tend to be perpendicular to each other across a planar (110) interface, a feature found in our previous simulations in agreement with experiment [28,29]. However, for Cr clusters bound by at least one (110) interface, we still find that a Col configuration represents the lowest-energy state. Moreover, all the NCol initial states decay to the Col ground state for most of the clusters, except for the octahedral clusters with $n = 15$ and 24, and the mixed clusters with $n = 22$, 41, and 70, where local minima with NCol arrangements of magnetic moments are found. The energy difference between the Col and NCol states [E(NCol) − E(Col)) of these clusters is fairly small: 0.09, 0.07, 0.04, 0.17, and 0.08 eV per cluster, respectively. A schematic representation of NCol structures is shown in Fig. 3, where all the magnetic moments are coplanar.

It is natural to attempt to rationalize magnetic behavior of the clusters in terms of magnetic frustration and the part played by Cr-Fe interfaces [28]. Coupling between Fe and Cr moments across a planar (110) interface results from competition between two tendencies resulting in magnetic frustration: the strong *nn* and *nnn* Fe-Cr AF coupling at the interface, and *nn* Cr-Cr AF coupling in the Cr lattice. For Cr clusters in iron, the situation becomes even more complicated, and size and shape dependent. When a cluster is relatively small and either all or most of the Cr atoms are situated at the interface, the "interface ordering tendency" of being antiparallel to the Fe moments clearly dominates over the Cr-Cr AF "bulk ordering tendency." This is indeed the case for the smallest N_{Cr} clusters ($N_{Cr} = 2$ to 6 and $n = 14$), where none of the Cr atoms have the local bcc-Cr-like environment

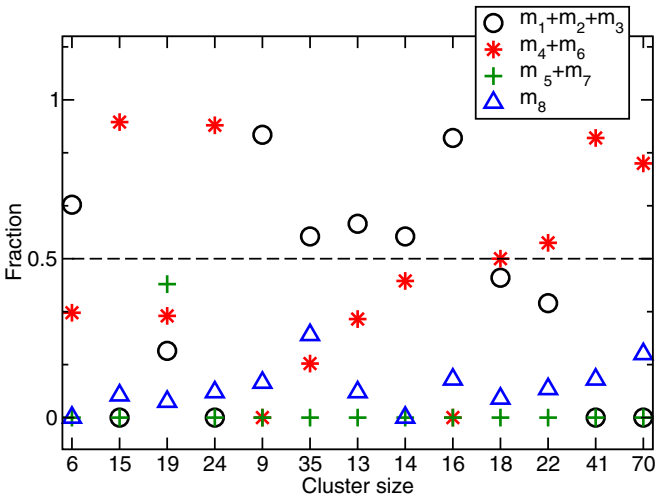

FIG. 4. (Color online) Fraction of Cr atoms (m_i) with i Cr nearest neighbors (nn) versus the size of the Cr cluster (N_{Cr}), for all the octahedral, cubic, and mixed clusters studied.

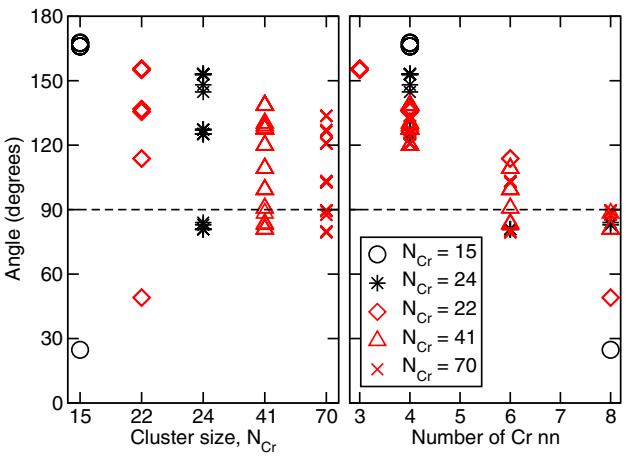

FIG. 5. (Color online) Absolute value of the angles between local Cr moments and Fe lattice moments in NCol N_{Cr}-cluster configurations (N_{Cr} = 15, 24, 22, 41, and 70) versus (left) cluster size, and (right) the number of Cr nn.

with all 8 of its nearest neighbors being Cr atoms. The fraction of Cr atoms in each cluster with i Cr nearest neighbors is shown in Fig. 4. For the medium-size clusters, where both interface and bulk tendencies are comparable, the induced magnetic frustration may potentially promote the formation of NCol structures. In practice, there is no simple rule for predicting the occurrence of a low-energy NCol state for medium-size clusters, which depends on the specific arrangement of Cr atoms. Within the range of cluster sizes considered here, we note from Fig. 4 that all the clusters characterized by a dominant fraction of atoms with either 4 or 6 Cr nn exhibit metastable NCol configurations ($N_{Cr} = 15, 24, 22, 41$, and 70). In these configurations, the local moments of Cr atoms in the smaller clusters ($N_{Cr} = 15, 22$) all show rather small deviations from collinearity with respect to the moments of Fe atoms. In the larger clusters with non-negligible fraction of bulklike Cr atoms, the local moments of the outer Cr atoms (with 4 Cr nn) show relatively small deviation from collinearity, whereas the moments of the inner Cr atoms have orientations almost perpendicular to the Fe moments (Fig. 5).

It is also worth mentioning that the local moments of Fe atoms remain practically unchanged, and remain ferromagnetically ordered, for all the Col and NCol Cr cluster configurations explored in this study. The variation of magnetic properties of Cr clusters as a function of cluster size can therefore be primarily correlated with the magnitude and orientation of Cr magnetic moments. For instance, the magnitudes of moments averaged over all the Cr atoms for all the clusters are shown in Table II. All the clusters, including those exhibiting a NCol local minimum in addition to the Col configuration, show particularly low average magnitudes of moments in the Col state, which is a signature of magnetic frustration. There are two ways for the clusters to partially release the frustration, either by developing NCol magnetic states or by reducing the magnitude of moments on the most frustrated Cr atoms while keeping all the Cr moments collinear with the Fe moments (Fig. 6). It appears that in the case of Cr clusters, it is the second alternative that is realized for the lower-energy states for all the clusters considered here. Table II also shows nonzero cluster magnetization caused by the dominance of Fe-Cr over Cr-Cr AF coupling in the small and medium-size Cr clusters.

Fe and Cr have very similar atomic volumes in bcc lattice, and the atomic-position relaxations of systems containing clusters are generally small. It is known that magnetism of Cr atoms is very sensitive to structural relaxations, variation of Cr atomic volume, and interatomic distances. We have found negligible effect of relaxation on magnetic moments for all the Cr clusters where NCol configuration was found to be neither stable nor metastable. For clusters with low-energy Ncol metastable states (containing 15, 22, 24, 41, 70 Cr atoms), we found a slight effect of relaxation reducing deviation from collinearity. In these cases, a typical angle variation of magnetic moments due to relaxation is around 10°, and the largest change noted is less than 20°.

B. Fe clusters in AF bcc Cr

Similarly to the case of Cr clusters in Fe, we now investigate the ground-state magnetic configurations of Fe clusters in AF bcc Cr. We consider small Fe clusters with $N_{Fe} = 2$ to 5 (Fig. 7), octahedral clusters with $N_{Fe} = 6$, 15, 19, and 24 (Figs. 8 and 10) with the same atomic structure as Cr clusters described in Sec. III A, and a cubic cluster containing 9 Fe atoms.

Before discussing Fe clusters, we note that magnetic frustration is already visible for an isolated Fe atom in AF bcc Cr. A substitutional Fe atom in AF bcc Cr is magnetically frustrated since the antiparallel-coupling preference for both the nn and nnn Fe-Cr pairs cannot be satisfied simultaneously. Again, there are two alternative ways to partially release magnetic frustration, that is, the Fe moment remains antiparallel to the moment of the nn Cr atoms and its magnitude decreases significantly, or it changes orientation and becomes noncollinear with respect to the Cr moments. The lowest-energy solution predicted by DFT is the former one, with a very small Fe moment of 0.21 μ_B (Fig. 9). This finding is consistent with the existing experimental data reported by

TABLE II. DFT average magnitude of magnetic moments of Cr atoms in clusters ($\langle M\rangle = \frac{1}{N_{\rm Cr}}\sum|\mathbf{M}_i|$), given in μ_B units, and the magnitude (in μ_B) of Cr cluster magnetization ($M^t = \frac{1}{N_{\rm Cr}}|\sum\mathbf{M}_i|$), shown as functions of cluster size $N_{\rm Cr}$ for the lowest-energy collinear (Col) and noncollinear (NCol) states. For the Col states, cluster magnetization is antiparallel to the Fe moments. For the NCol states, the angle between the cluster magnetization and Fe moments varies between 176° and 180°.

	6	15	19	24	9	35	13	14	16	18	22	41	70
$\langle M\rangle$ (Col)	1.23	0.51	1.03	0.52	1.97	1.45	0.97	1.62	1.02	0.95	0.62	0.48	0.67
$\langle M\rangle$ (NCol)		0.53		0.69							0.84	0.85	0.95
M^t (Col)	0.96	0.46	0.65	0.43	1.61	0.94	0.64	0.98	0.86	0.72	0.52	0.36	0.26
M^t (NCol)		0.47		0.44							0.54	0.37	0.29

Dubiel *et al.* [42]. There is also a metastable NCol magnetic state with a slightly increased local moment (0.87 μ_B). This state is only 0.04 eV per cluster higher in energy, where the angles between the Fe moment and *nn* and *nnn* Cr moments are 114° and 66°, respectively (Table III). Based on theoretical predictions [27,40], we know that it is always energetically more favorable for Fe atoms to form clusters than to stay isolated in the Cr lattice. It is expected that the very strong magnetic frustration of single Fe atoms, reflected by their much smaller local moment compared with the Fe moments in clusters (Fig. 9), contribute to this preference to cluster.

In comparison with Cr clusters in ferromagnetic Fe, more energy minima corresponding to distinct magnetic states are found for Fe clusters in AF Cr. This may be rationalized by noting that magnetism of Cr atoms is highly sensitive to neighboring Fe atoms, in other words, it is largely determined by the local chemical environment. On the other hand, magnetism of Fe clusters is mainly determined by strong Fe-Fe FM coupling, and hence it is less sensitive to interaction with Cr atoms. Moreover, in bcc lattice, Fe shows stronger tendency to becoming magnetic than Cr, attested by a larger energy difference between FM and NM (nonmagnetic) states of Fe (0.54 eV/atom) compared to a much smaller difference between AF and NM states of Cr (0.03 eV/atom) [20]. Such differences are directly reflected in the magnitudes of local moments on Cr and Fe atoms in the respective clusters. In Cr clusters, the magnitudes of local moments often differ significantly between atoms in a cluster and between different clusters (see Table II and Fig. 6). On the other hand, the magnitudes of atomic moments on all the atoms in a Fe cluster are fairly similar, and the average magnitude of atomic moment in a cluster converges already to the magnitude of bcc bulk Fe moment (2.25 μ_B) even for relatively modest cluster sizes (Fig. 9). Such differences between Fe and Cr are expected to result in dissimilar behavior of Fe and Cr clusters, especially if some of the atoms are magnetically frustrated. In general, Fe atoms develop NCol configurations much more readily, as shown below, whereas Cr atoms tend to adopt collinear configurations characterized by fairly small atomic moments. We have also found that magnetic moments are coplanar in all the low-energy NCol configurations of clusters that we studied here.

We consider three possible magnetic configurations of a Fe dimer ($N_{\rm Fe} = 2$): (i) the two Fe moments are parallel to each other and collinear to the Cr moments, (ii) moments of the two Fe atoms are antiparallel to each other, and both are antiparallel to the moments of their respective *nn* Cr atoms, and (iii) the two Fe moments are noncollinear with respect to each other and moments on the Cr lattice. The latter configuration is in fact the lowest-energy state, exhibiting the largest atomic moments. The first and second configurations are, respectively, 0.04 and

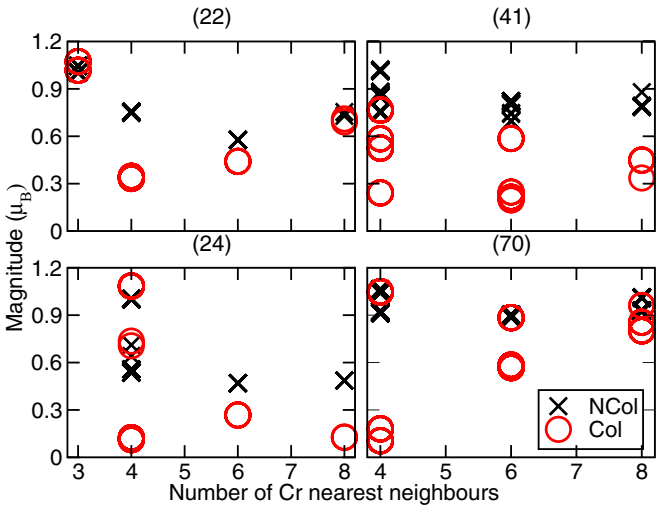

FIG. 6. (Color online) Magnitudes of local moments on atoms in Col and NCol configurations of *n*-Cr clusters versus the number of Cr *nn*.

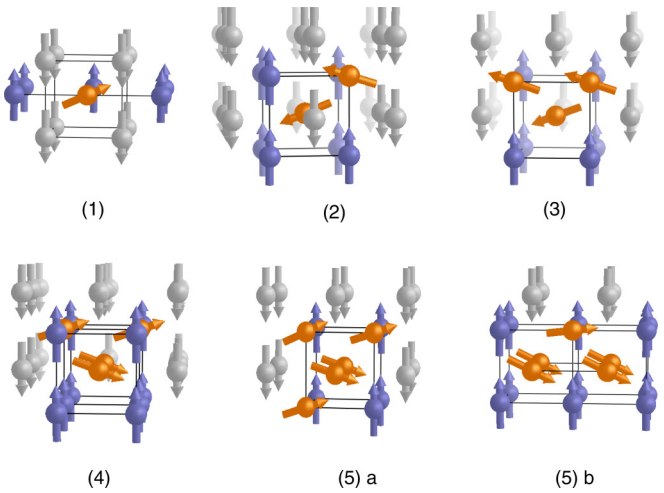

FIG. 7. (Color online) Schematic representations of atomic positions and magnetic moments (arrows) for the lowest-energy NCol state of a single Fe atom and small Fe clusters in AF bcc Cr. Yellow and gray spheres denote Fe and Cr atoms, respectively. Fe cluster sizes $N_{\rm Fe}$ are given in parentheses.

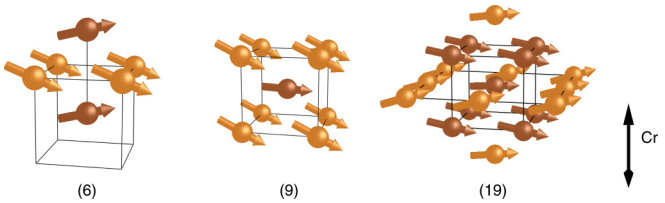

FIG. 8. (Color online) Schematic representations of atomic positions and magnetic moments (arrows) for the lowest-energy NCol state of Fe clusters with $N_{Fe} = 6$, 9, and 19 in AF bcc Cr. Fe cluster sizes (N_{Fe}) are given in parentheses. Orientations of AF-ordered moments of Cr atoms are shown by the up-down arrow.

0.07 eV above the ground state. The average magnitudes of Fe moments for the three cases are, respectively, 1.34 μ_B, 0.30 μ_B, and 1.89 μ_B. Note that states (i) and (ii) favor FM coupling between the two Fe atoms and AF coupling between the *nn* Fe-Cr pairs. The NCol configuration [state (iii)] gives the best compromise between all the FM Fe-Fe, and *nn* and *nnn* AF Fe-Cr magnetic interactions. In this NCol state, the angle between the two Fe local moments is 39°, whereas the angles between the Fe moment and the moments of their respective Cr *nn* are 107° and 112° (Table III).

In comparison with Cr clusters in Fe, all the small Fe clusters in Cr studied here, with $N_{Fe} = 2$ to 5, exhibit noncollinear magnetic configurations as the lowest-energy states. Energy differences per cluster between the lowest-energy collinear and noncollinear states are 0.06, 0.09, 0.07, and 0.05 eV, respectively, for the 3-, 4-, 5a-, and 5b-clusters shown in Fig. 7. In these clusters, all the Fe atoms have at least four Cr *nn*. As was noted in relation to a Fe dimer, noncollinear arrangements allow us to reconcile, as much as possible, the competing magnetic coupling tendencies between the neighboring Fe-Fe and Fe-Cr pairs. The resulting atomic moment orientations are also similar to the Fe dimer case, that is, local moments on the Fe atoms are at an angle of up to 39°

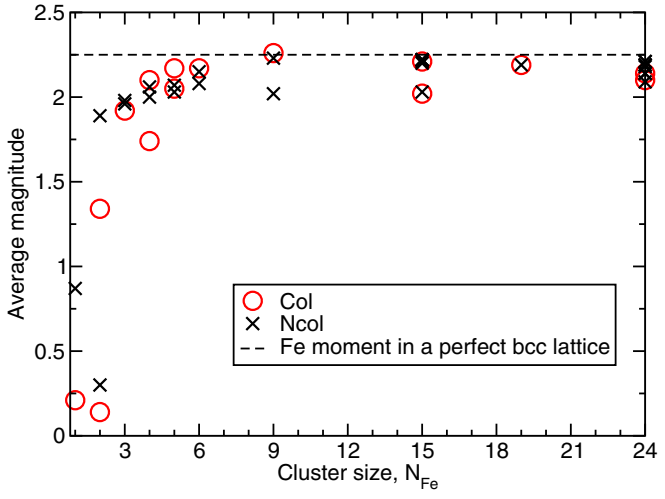

FIG. 9. (Color online) Average magnitude of local magnetic moments (in μ_B units), computed for various Col and NCol configurations, shown for all the Fe clusters included in this study. Magnitude of a Fe atom moment in bcc FM lattice is shown for comparison.

TABLE III. Angles between Fe atomic moments in the clusters and Cr *nn* moments for various Fe cluster sizes (N_{Fe}). Results of DFT and MCE calculations are given for comparison. Cluster configurations are shown in Figs. 7 and 8. The number of Fe atoms with the same orientation of moments is shown in parentheses. For the 5-atomic cluster (a), the distance between the first pair of equivalent atoms is a; the distance between the second pair of equivalent atoms is $a\sqrt{2}$. For the 19-atomic cluster, the first four equivalent atoms are situated at the vertices of an octahedron; the second four equivalent atoms are at the center of its egdes. The angle for the central atom in the 9- and 19-atom clusters is defined with the same reference as for its 8 Fe *nn* neighbor atoms.

N_{Fe}	Angle (deg), DFT	Angle (deg), MCE
1	114	130
2	107, 112	117
3	109(2), 110	127(2), 109
4	110(4)	117(4)
5a	108(2), 108(2), 113	118(2), 136(2), 163
5b	96, 116(4)	91, 139(4)
6	103(2), 112(4)	99(2), 129(4)
9	116(8), 93(central)	153(8), 174(central)
19	107(8), 101(4), 101(4), 97(2), 87(central)	121(8), 114(4), 126(4), 110(2), 154 (central)

with respect to each other, and at angles varying from 108° to 116° with respect to the *nn* Cr moments (Table III). The central atom in a 5-Fe cluster in (b) configuration (Fig. 7) presents a particularly frustrated case. The moment of this Fe atom is nearly perpendicular (the angle is 96°) to the moments of its four Cr nearest neighbors.

Noncollinear magnetic ground states gradually vanish as the size of an Fe cluster increases. In terms of competition between Fe-Fe FM and Fe-Cr AF coupling tendencies, the former becomes dominant in the limit of large cluster size. Consistently, we find that collinear states are either very close or lower in energy than the noncollinear states. For instance, for a cubic cluster with $N_{Fe} = 9$, and for octahedral clusters with $N_{Fe} = 6$ and 19, the energetically most favorable noncollinear states (Fig. 8) are only 0.03, 0.01, and 0.02 eV per cluster lower in energy than the corresponding collinear states. These energy differences are within the uncertainty margin of DFT calculations. Therefore, in practice the Col and NCol states can be treated as degenerate. In the NCol states, the maximum angles between Fe moments are 35°, 23°, and 18°, respectively, for the 6-, 9-, and 19-Fe clusters. The angles between Fe and *nn* Cr moments are given in Table III, varying from 97° to 116°, similar to the smaller cluster cases.

For other medium-size but more compact clusters ($N_{Fe} =$ 15 and 24), where all the Fe atoms have at least, and in most cases, four Fe *nn*, the FM coupling between Fe atoms dominates. Consequently, the lowest-energy state is a collinear configuration, where most of the Fe atoms (9 over 15 and 14 over 24) are not magnetically frustrated with respect to their *nn* Cr atoms, as shown in the left plots of Fig. 10. Many noncollinear states exist as local energy minima, obtained with different magnetic-moment initializations of DFT calculations. Relative energies of such states are shown in Fig. 11. Note that many of the NCol states, with a rather

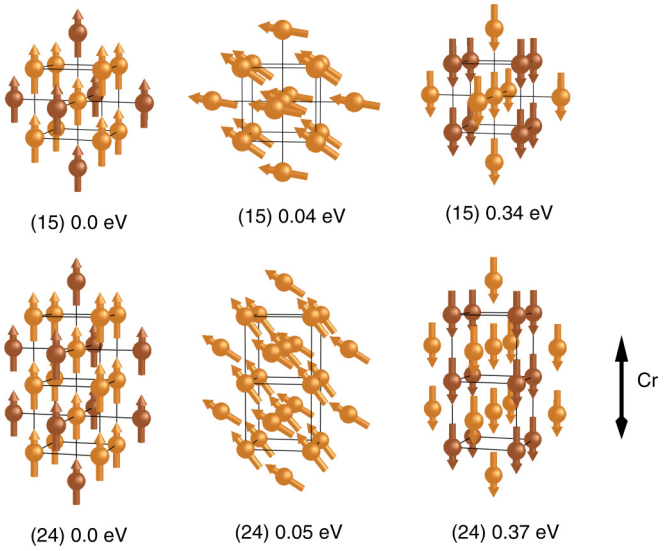

FIG. 10. (Color online) Schematic representation of atomic positions and local magnetic moments (arrows) of Fe clusters of 15 and 24 atoms in AF bcc Cr. Two Col (left and right) and an intermediate-energy NCol (middle) configurations are shown together the difference between their energy, per cluster, and that of the ground state. In the Col states, the light yellow atoms have local moments antiparallel to their *nn* Cr atoms. The Fe cluster size is given in parentheses. Orientation of the lattice Cr atoms is also shown.

weak deviation from collinearity, are less than 0.05 eV above the Col ground state. Therefore, there is high probability of such noncollinear states being occupied even at very low temperatures.

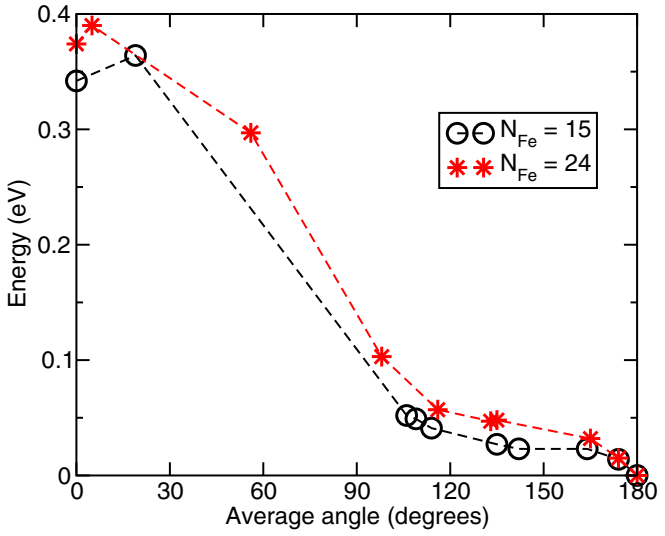

FIG. 11. (Color online) 15- and 24-Fe clusters in AF bcc Cr: energy per cluster of a magnetic configuration with respect to the magnetic ground state, computed for various Col and NCol states versus the average angle of Fe local magnetic moments. States with angle = 180° and 0° correspond to Col states shown on the left and right panels of Fig. 10, respectively.

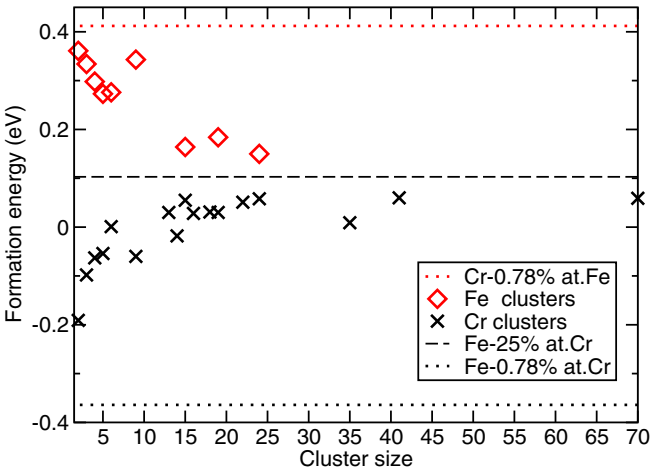

FIG. 12. (Color online) Formation energy per cluster atom [as defined in Eq. (1)] of a Fe or a Cr atom forming a cluster compared with the formation energy of an atom of the same species in either a dilute or a concentrated random solid solution.

Formation energy per cluster atom, as defined by Eq. (1), is calculated and shown in Fig. 12, for a Fe or a Cr atom in a cluster. They are also compared with the formation energy of an atom of the same species in either a dilute (0.78 at. % of solutes) or a concentrated (25 at. % of Cr) random solid solution.

The general trends exhibited by the formation energy of a cluster atom as a function of cluster size are beyond the scope of the present DFT data since they are only limited to rather small-size clusters. They will be further discussed on the basis of MCE data in Sec. IV.

While still discussing the DFT data, we note that the formation of Fe clusters is always energetically favorable, compared with the random dilute solution of Fe in Cr. This is consistent with the fact that the mixing energies of Fe-Cr alloys on the Cr-rich side are positive, confirming the tendency of alloys towards phase separation [6,27]. Among the clusters studied here, the 9-Fe cubic cluster appears to have larger energy compared with other clusters of similar size, particularly the octahedral clusters with 6 and 15 Fe atoms. Note that the 9-Fe cluster is a particularly open cluster, where a majority of Fe atoms (8 over 9) have only 1 Fe *nn*. Unfortunately, the relatively limited amount of DFT data do not make it possible to draw a general conclusion about the relation between the energy of a cluster and its geometry.

As shown in Fig. 12, the formation energy of a Cr atom in a cluster is expectedly higher than the corresponding value for a Cr atom in a dilute-Cr solid solution, but lower than the corresponding energy in a 25 at. % Cr random solution. Again, these results are fully consistent with the Fe-Cr mixing energies, which show negative values on the dilute-Cr side and positive above 10–15 at. % Cr [6,7,27], indicating a transition from chemical ordering to the phase separation (and precipitation) tendency. As already mentioned previously [6,7,27], these tendencies are closely linked to magnetic properties of Fe-Cr solid solution, that is, Cr atoms in an extremely dilute alloy are stabilized by the induced magnetic moments, while at higher Cr concentration in a random alloy,

magnetic frustration emerges as the number of neighboring Cr atoms increases.

It is also interesting to note that the two cubic clusters containing 9 and 35 Cr atoms have lower energies compared with other clusters of similar size. This is consistent with the larger averaged magnetic moment of these cubic clusters (Table II), due to the presence of a dominant fraction of Cr atoms with mainly Fe *nn* (Fig. 4). On the other hand, the most magnetically frustrated clusters containing 15, 22, 24, 41, and 70 Cr atoms discussed above, which all exhibit low averaged magnetic moments (Table II) and NCol metastable states, have rather high formation energies.

IV. MCE RESULTS AND DISCUSSION

A. Cr clusters in Fe

In this section, we investigate equilibrium magnetic structures of Cr clusters in Fe matrix using magnetic cluster expansion simulations [19,30]. When choosing the structure of clusters, we explored all the clusters investigated by DFT in the preceding sections of the paper. Also, we studied larger clusters that cannot be treated using the relatively small DFT supercells. The two types of such larger clusters are the cubic clusters with six (100) interfaces and octahedral clusters with eight (110) interfaces. Using the notations of Table I, a cubic cluster can be represented as $2n-1$ layers with a general formula $n^2-(n-1)^2-n^2-\ldots-(n-1)^2-n^2$, where the total number of atoms is $n^3+(n-1)^3$. For the octahedral clusters with (110) interfaces the general formula is $1^2-2^2-\ldots-n^2-(n-1)^2-\ldots-1^2$, with the total number of atoms in the cluster being $(2n^3+n)/3$. For the cubic clusters, the following sizes were included in the MCE simulation set: 9, 35, 91, 189, 341, 559, 855, and 1241 Cr atoms in Fe matrix. Octahedral clusters of size 6, 19, 44, 85, 146, 231, 344, 489, 670, 891, 1156, and 1469 Cr atoms in Fe matrix were also included in the MCE study. Simulations were performed using a supercell containing 16 000 atoms ($20\times20\times20$ bcc unit cells) for both types of clusters.

To compare MCE simulations with DFT calculations, extensive searches for a global minimum as well as for possible metastable magnetic configurations were conducted. Simulations were performed assuming that moments change their directions, and also with moments constrained to collinearity. Since the energy difference between noncollinear and collinear magnetic configurations can be very small, especially for small Cr clusters, a three-stage quenching was performed from temperature $T=1000$ to $T=1$ K (first stage), 10^{-3} K (second stage), and 10^{-6} K (third stage).

Summarizing the results, we found that in small clusters Cr atoms retain collinearity with respect to the Fe environment. Simulations with and without the collinearity constraint converged to the same (collinear) configurations for clusters containing up to 5 atoms, as well as for 6-atomic octahedral and 9-atomic cubic cluster. All the clusters with 13 and more Cr atoms studied here have noncollinear magnetic ground states. The ground-state configuration (collinear or noncollinear) and the energy difference between it and the higher-energy magnetic configuration are given for some clusters in Table IV both for MCE and DFT simulations. We note that the accuracy of the MCE parametrization is about 11 meV/atom [19]. However, in the case of larger clusters, only the surface atoms contribute to the overall error of an MCE simulation. In Table IV, we consider smaller clusters with the relative energy difference of less than 12 meV per cluster atom as practically degenerate between noncollinear and collinear magnetic states (they are denoted as DG in the table). For larger clusters with a significant number of atoms in the interior of the cluster, the difference of 5 meV per atom or even less makes it acceptable to consider a noncollinear magnetic state as the true ground state. Satisfactory agreement is found between the data derived from both methods. In particular, there are no stable or metastable noncollinear states, and collinear magnetic configurations represent the ground states of the smallest clusters. Magnetic noncollinearity emerges as the cluster size increases.

TABLE IV. Ground states (GS) and relative energies (in meV/atom) of the lowest-energy collinear and noncollinear magnetic configurations found for small clusters studied by both MCE and DFT methods. Here, DG refers to a state that is practically degenerate with respect to the ground state, where the degeneracy criterion is that the energy difference between the two states is within the uncertainty interval of simulations.

	Cr clusters				Fe clusters			
	MCE		DFT		MCE		DFT	
Cluster size	Col	NCol	Col	NCol	Col	NCol	Col	NCol
1	GS	Unstable	GS	Unstable	32.3	GS	GS	43.0
2	GS	Unstable	GS	Unstable	115.4	GS	20.0	GS
3	GS	Unstable	GS	Unstable	159.6	GS	20.0	GS
4	GS	Unstable	GS	Unstable	52.3	GS	22.5	GS
5	GS	Unstable	GS	Unstable	29.4	GS	10.0	GS
6	GS	Unstable	GS	Unstable	158.4	GS	DG	GS
9	GS	Unstable	GS	Unstable	10.9	GS	DG	GS
13	DG	GS	GS	Unstable	132.2	GS		
14	20.5	GS	GS	Unstable	40.3	GS		
15	DG	GS	GS	6.0	97.8	GS	GS	DG
16	DG	GS	GS	Unstable	84.3	GS		
18	DG	GS	GS	Unstable	72.1	GS		
19	24.5	GS	GS	Unstable	106.0	GS	DG	GS
22	DG	GS	GS	1.8	90.4	GS		
24	DG	GS	GS	2.9	69.7	GS	GS	DG
35	DG	GS	GS	Unstable	11.2	GS		
41	5.4	GS	GS	4.1	68.2	GS		
70	7.2	GS	GS	1.1	58.2	GS		

In magnetic cluster expansion simulations, the energy difference between a noncollinear ground state and a ground state found with collinearity constraint applied is the lowest for cubic clusters. For the octahedral and mixed clusters, the difference between the energies is larger, approaching 24.5 meV per Cr atom for a 19-atom cluster (Fig. 13). Such large difference is related to the large share of strongly (with respect to pure Cr) decreased chromium moments in the MCE collinear state of this cluster, as well as in the Col mixed 14-atomic cluster (Table IV). As we discuss in the following (see Sec. IV B), the error for the small moments may be substantially higher than the average accuracy of the MCE fit.

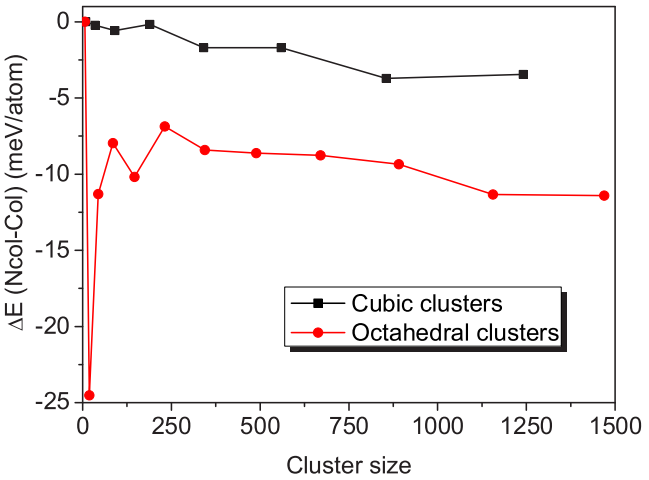

FIG. 13. (Color online) Energy difference between a non-collinear ground state and a ground state found using the collinearity constraint for cubic and octahedral chromium clusters, in meV per Cr atom.

The emergence of magnetic noncollinearity in cubic clusters is illustrated in Fig. 14, where we plot two components of magnetic moments of Cr atoms, parallel and orthogonal to bulk Fe atoms for the three smallest cubic clusters. For a 9-atom cluster, moments are completely collinear to the Fe moments.

The dependence of the tilt angle (with respect to the direction of bulk Fe magnetization) and the magnitude of Cr moments on the number of their nearest Cr neighbors for small cubic and octahedral clusters (35 and 44 Cr atoms, respectively) is shown in Fig. 15. According to Fig. 15(a), the moments of atoms with fewer than three Cr atoms in the nearest-neighbor shell are almost completely collinear and antiparallel to the moment of iron lattice. Strong deviation from collinearity is found for atoms with four nearest Cr neighbors in cubic, and with five Cr neighbors in octahedral clusters, respectively. Atoms that are inside the two clusters and have

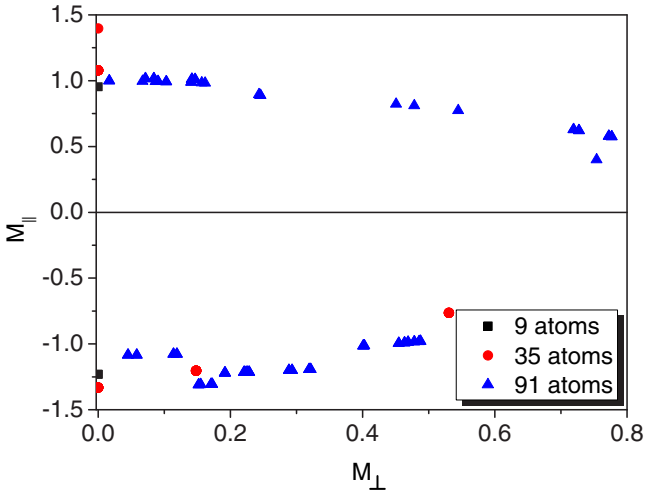

FIG. 14. (Color online) Parallel and orthogonal components of Cr magnetic moments (in μ_B) computed for the three smallest cubic clusters investigated by MCE.

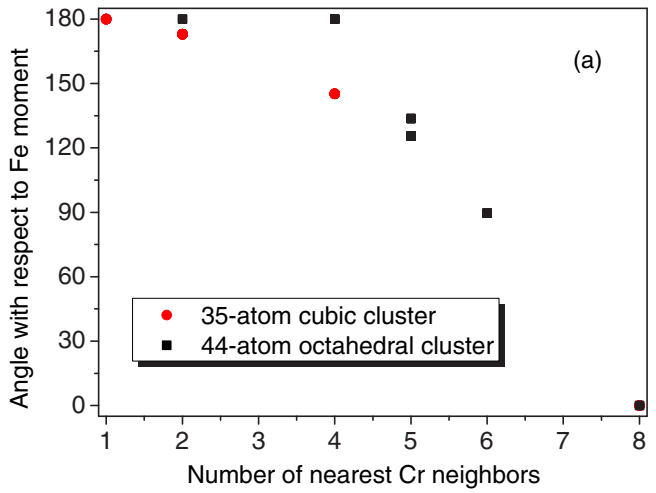

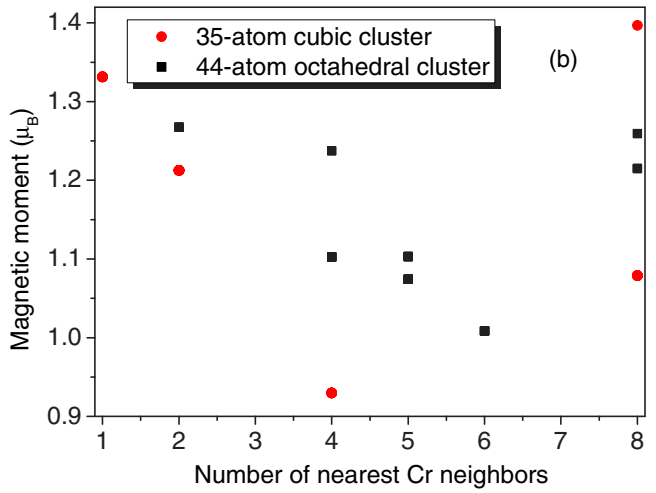

FIG. 15. (Color online) Angle (in deg) between Fe magnetic moment and moments of Cr atoms in small cubic and octahedral clusters plotted as a function of the number of nearest Cr neighbors (a). The magnitude of magnetic moment of Cr atoms in small cubic and octahedral clusters plotted as a function of the number of nearest Cr neighbors (b).

8 Cr among their nearest neighbors are strongly influenced by the large number of collinear Cr atoms at the cluster-matrix interface and hence are close to collinearity themselves, with their moments being almost parallel to the moments of iron atoms. The magnitude of magnetic moment is minimum for atoms with four to six nearest Cr neighbors [Fig. 15(b)]. This reduction of the local moment coincides with strong tilting away from collinearity and represents another way of releasing magnetic frustration, similar to the one found in DFT studies of Fe clusters in Cr (see above, Sec. III B). In the interior region of Cr clusters, the magnitude of magnetic moments of Cr atoms increases.

Magnetic moments of Cr atoms in the clusters for which noncollinear solutions were also found in DFT calculations are shown in Fig. 16, in order to compare with the DFT magnetic configurations (Fig. 3). They all are found to be noncollinear in MCE simulations. Energy gains of noncollinear compared to collinear magnetic configurations are 4.2, 0.4, 1.0, 5.4, and 7.2 meV per Cr atom for 15, 22, 24, 41, and 70 atomic clusters,

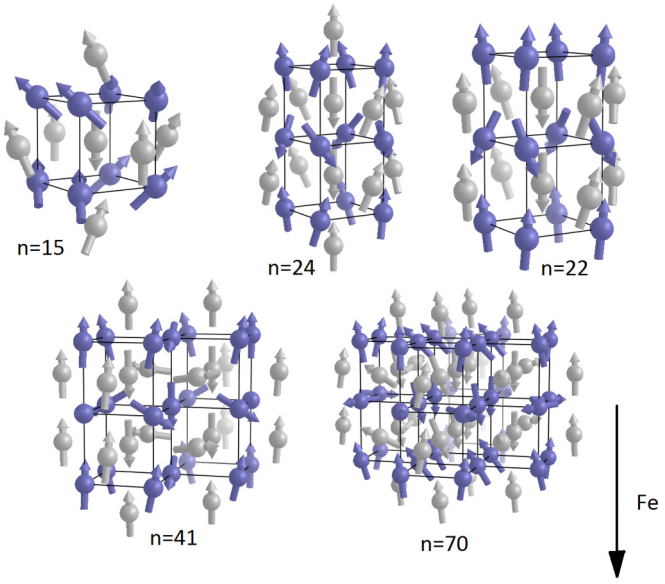

FIG. 16. (Color online) Schematic representation of atomic positions and local magnetic moments (arrows) of Cr clusters containing 15, 24, 22, 41, and 70 atoms found in MCE simulations. Orientation of the FM-ordered Fe moments is also shown.

respectively. Again, for smaller clusters with almost all the atoms being at the surface (15, 22, and 24 atomic clusters), collinear and noncollinear magnetic configurations should be considered as practically degenerate.

Variation of magnetic moments of Fe atoms at the Cr cluster interface was also investigated. In the vicinity of Cr clusters, iron moments are smaller than in the bulk, in agreement with our analysis of Fe/Cr interfaces [28] and calculations by Alvarado *et al.* [43].

The formation energy of Cr clusters calculated according to Eq. (1) is shown in Fig. 17. A single chromium atom has

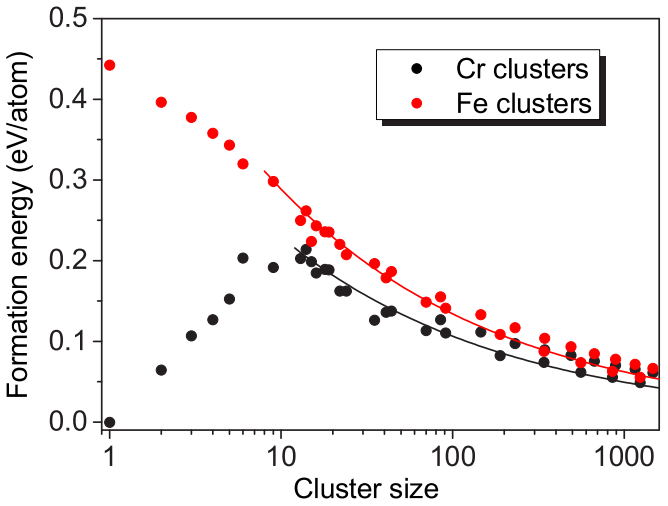

FIG. 17. (Color online) Formation energies of Cr and Fe clusters as functions of cluster size (meV per cluster atom). For large clusters, the formation energy decreases in proportion to the relative number of atoms at the interface (which is proportional to $n^{-1/3}$, as shown by solid lines).

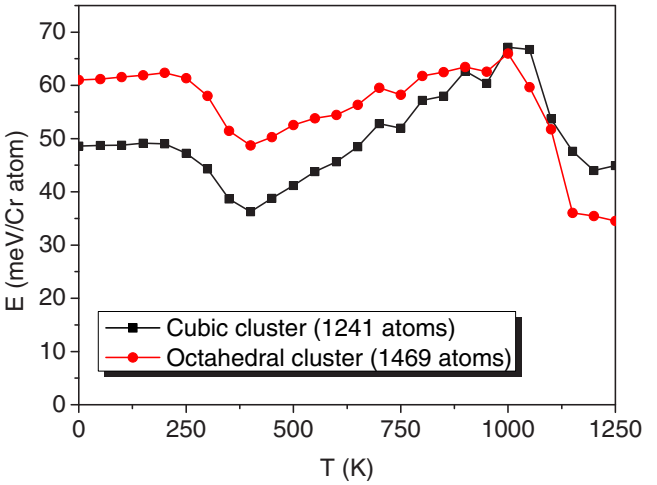

FIG. 18. (Color online) Formation energy, per Cr atom, of chromium clusters (1241-atomic cubic cluster and 1469-atomic octahedral cluster) plotted as a function of temperature.

negative energy in agreement with the fact that Cr is fully soluble in bcc Fe in the low-concentration limit. However, with the increasing cluster size the formation energy becomes positive and also increases because of magnetic frustration. For large clusters, the formation energy is mainly the energy of Fe/Cr interfaces and decreases as the relative number of atoms at the interface decreases [44]. As a result, the formation energy per atom has a maximum at the cluster sizes of 10 to 20 atoms. We note that, in general, cubic clusters have lower formation energy than the octahedral clusters of similar size.

Temperature dependence of cluster energy for large cubic and octahedral chromium clusters is shown in Fig. 18. Results are normalized to a single cluster atom. We see that the energy plotted as a function of temperature shows the same features that were found for Fe-Cr interfaces, namely, that it decreases at temperatures corresponding to magnetic transitions, the Néel temperature of Cr (310 K) and the Curie temperature of Fe (1043 K). Also, the relative energies of cubic and octahedral clusters follow the trend shown in Fig. 12 of Ref. [28], namely, that an octahedral cluster with (110) interfaces has higher energy per Cr atom at low temperatures, but the relative stability of octahedral and cubic [with (100) interfaces] clusters changes near the Curie transition temperature.

Because of antiferromagnetic coupling between Fe and Cr moments at the cluster-matrix interface, ferromagnetic iron matrix induces nonvanishing magnetization in chromium clusters. For small clusters, the average moment per Cr atom can be as high as $1\mu_B$, i.e., it approaches the magnitude of magnetic moment of pure bcc Cr. We investigated the dependence of this quantity on the cluster size as well as on temperature. The cluster size dependence of cluster magnetization, per Cr atom, is similar for cubic and octahedral clusters, as seen in Fig. 19. If the cluster magnetization, treated as a function of cluster size n, were proportional to the fraction of Cr atoms at the cluster surface ($\sim n^{2/3}$), magnetization per Cr atom varies approximately as $n^{-1/3}$. Our fit gives the power law for magnetization (per atom) very close to $n^{-2/5}$ (the exponents being -0.40652 for the cubic and -0.42058 for the octahedral clusters, respectively), showing that in fact

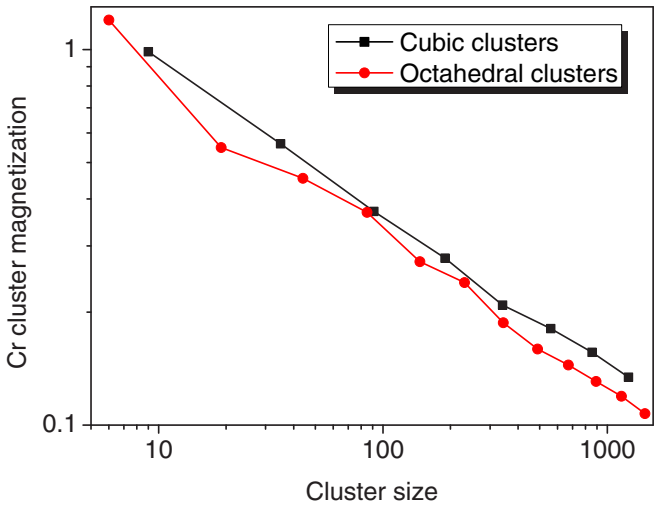

FIG. 19. (Color online) Magnetization (in μ_B) of Cr clusters, per atom, plotted vs cluster size for cubic and octahedral clusters.

magnetization decreases slightly faster than $n^{-1/3}$. The total induced magnetization of a cluster varies as a function of the number of atoms in the cluster as $n^{3/5}$. Magnetization of Cr clusters induced by the surrounding Fe atoms vanishes only at high temperature, comparable with the Curie temperature of Fe (see Fig. 20).

To investigate the temperature dependence of magnetic properties of clusters, we analyzed the nearest-neighbor Cr-Cr antiferromagnetic correlations, defined as

$$C_{nn} = \frac{1}{N_{nn}} \sum_{i,j \in nn} \frac{\mathbf{M}_i \cdot \mathbf{M}_j}{|\mathbf{M}_i||\mathbf{M}_j|}. \tag{3}$$

For cubic clusters, correlation function C_{nn} is shown in Fig. 21 together with the correlation function computed for pure Cr. For the relatively small 189-atom cluster correlations are not very strong, but they persist until relatively high temperatures, higher than the Néel temperature of Cr. This is due to the

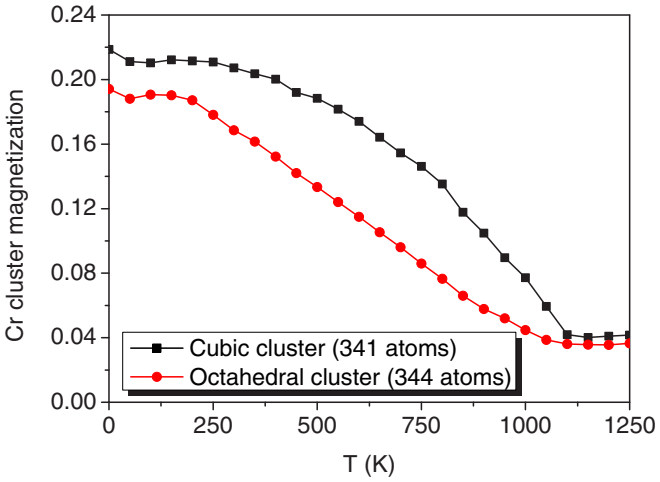

FIG. 20. (Color online) Temperature dependence of magnetization (in μ_B) of cubic (341 atoms) and octahedral (344 atoms) Cr clusters.

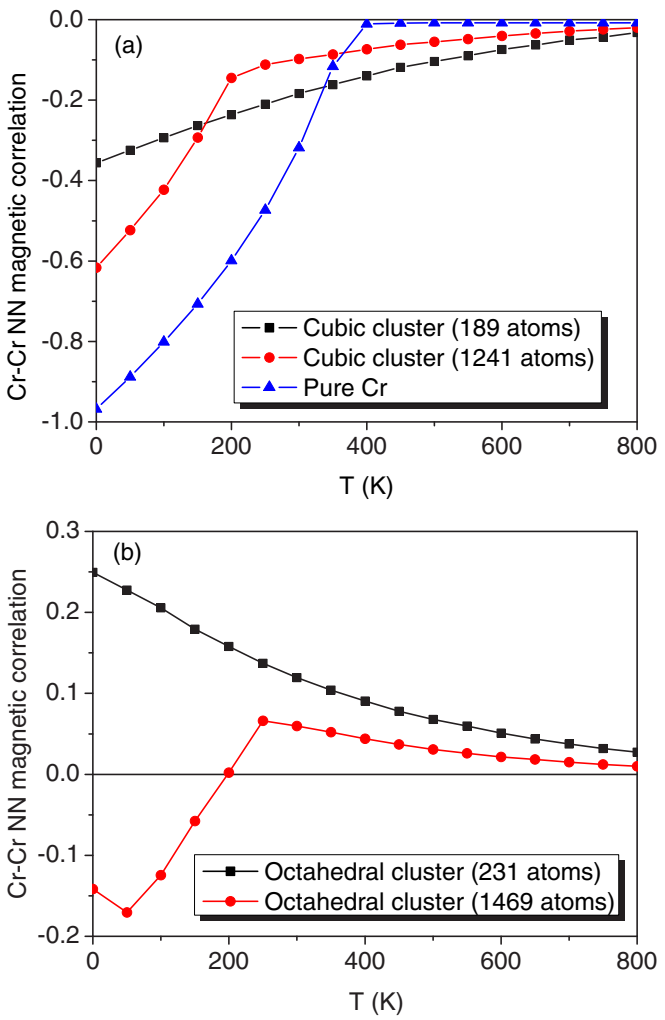

FIG. 21. (Color online) Antiferromagnetic correlations in cubic Cr clusters (a) and octahedral Cr clusters (b).

antiferromagnetic coupling of atoms at the cluster interface with the Fe matrix, which helps preserve magnetic order inside the cluster even at high temperatures. For the large 1241-atom cluster, correlations at low temperatures are stronger, but they decrease faster with temperature. This behavior is closer to what is found for pure chromium. Temperature dependence of correlations is more interesting in octahedral clusters [Fig. 21(b)]. For a small 231-atom cluster, correlations turn out to be positive in the entire range of temperatures. For the large 1469-atom cluster, correlations are antiferromagnetic at low temperatures, but they change sign at temperatures close to the Néel temperature of Cr. This unusual behavior can be explained if we note that in octahedral clusters, unlike in cubic clusters, there is a large fraction of nearest-neighbor bonds between pairs of Cr atoms situated at the interface between the cluster and the matrix (in cubic clusters, there are no such bonds). In a 231-atom octahedral cluster, 576 out of 1256 (45.9%) nearest-neighbor bonds involve interfacial atoms, whereas for the 1469-atom cluster the fraction is 2304 out of 9432 (24.4%). Interfacial Cr atom moments prefer antiparallel orientations of magnetic moments with respect to the Fe matrix, and as a result they are parallel to each other, despite the

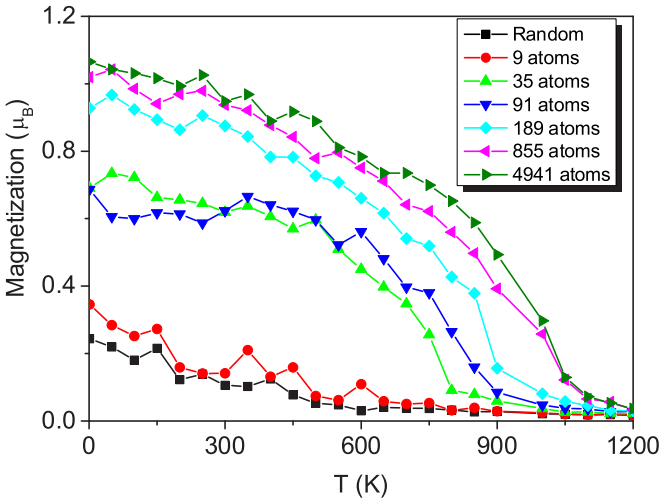

FIG. 22. (Color online) Magnetization, plotted as a function of temperature, for Fe-40 at. % Cr alloys. Chromium atoms are either distributed randomly in Fe matrix, or form a mixture of cubic nanoclusters of various sizes suspended in Fe-12 at. % random alloys (see text).

fact that Cr-Cr interactions are antiferromagnetic (AF). This effect manifests itself stronger in smaller clusters, but even in a large 1469-atom cluster, the AF Fe-Cr interaction dominates over the AF Cr-Cr interaction near the Néel temperature of Cr.

In order to study how magnetization of an alloy with high Cr content depends on both temperature and solute cluster size, we performed simulations for several Fe-Cr systems, consisting of a mixture of cubic chromium clusters and random Fe-Cr alloy. The configurations were created as follows: for a given cluster size, Cr clusters were randomly distributed in the simulation box. The rest of the box contained Fe-12 at. % Cr random solution. The total amount of chromium atoms in the system was kept at 6400, corresponding to 40 at. % Cr. Also, fully random Fe-40 at. % Cr mixture was investigated. Figure 22 shows the temperature dependence of magnetization for a random alloy and alloys with different cubic cluster sizes, starting with 566 9-atom Cr clusters and finishing with a single cluster consisting of 4941 Cr atoms. The Fe-Cr random mixture and alloy containing 9-atom clusters show almost identical temperature dependence, with magnetization approaching zero at about 600 K. For larger 35- and 91-atom Cr clusters, low-temperature magnetization is higher and it vanishes at higher temperatures of 800–900 K. Finally, starting from 189-atomic clusters, the magnetization behavior changes only slightly with increasing clusters size, and magnetization vanishes entirely at temperatures that are close to the Curie temperature of pure iron (1043 K).

Results shown in Fig. 22 can be discussed in relation to the experimental study by Yamamoto [18], although a direct comparison is hardly possible. Figure 3 of Ref. [18] shows variation of magnetization versus temperature for several Fe-Cr specimens quenched from 1100 °C and annealed at 500 °C. For specimens with more than 38 wt.% Cr, the difference between magnetization curves is very prominent. The quenched specimens show a sluggish decrease of magnetization with temperature, while for the annealed specimens, a sharp drop in magnetization is observed above 550 °C (820–830 K). Yamamoto [18] attributes this sharp drop to a phase transformation in Fe-Cr, presumably a transition from a clustered to a random solution phase above the miscibility gap. In our simulations, this would correspond to a sharp transition from the plots corresponding to large (189 and more Cr atoms) clusters in Fig. 22 to a plot corresponding to a completely random solution, with the corresponding rapid decrease in magnetization. On the other hand, heating of a quenched system with 46.5 wt.% Cr results in, according to Ref. [18], (i) a Curie transition at 380° C (close to our prediction of 600 K for a random alloy) and (ii) diffusion-driven precipitation of chromium at higher temperature, resulting in the complete disappearance of magnetization above 550 °C, like in the case of annealed specimens. A direct comparison between experiment and simulations is not possible since in simulations, the thermally activated diffusion of Cr atoms is not taken into account (Cr atoms do not change position in the simulation cell).

Overall, magnetic noncollinearity of Cr clusters in Fe appears to have the same origin as the noncollinearity found at Fe/Cr interfaces [28], namely, that it results from magnetic frustration occurring as a result of competition between the antiferromagnetic *nn* and *nnn* Fe-Cr interactions and antiferromagnetic *nn* Cr-Cr interactions. However, in Cr clusters the picture is more complex than at interfaces because in clusters there is a preferred direction along which magnetization and other properties change (at an interface, such direction is provided by the vector normal to the interface). In a cluster, the magnetic state of each Cr atom depends on its distance from several interfaces, and a simple model developed in [28] as a criterion of magnetic noncollinearity cannot be directly applied here.

B. Fe clusters in Cr

Comparison of MCE and DFT results for the angles of Fe moments in small clusters and the surrounding Cr moments is presented in Table III. For a single Fe atom in Cr, MCE predicts a NCol ground state where the angle between Fe magnetic moment and Cr moments is about 130°. This is very close to the corresponding noncollinear DFT solution (114°). Energy gain of noncollinear configuration relative to the collinear one for a single Fe atom is 32 meV, which is much less than for the two- and three-atomic clusters (see Table IV). The magnitude of Fe magnetic moment in both noncollinear and collinear solutions is reduced in comparison with bulk iron, but not as strongly as in the DFT calculations: the moment of an Fe atom is 1.584 μ_B in the noncollinear and 1.480 μ_B in the collinear magnetic configurations. In our opinion, the difference between DFT and MCE ground states (collinear versus noncollinear) in this case is related to the drastic decrease of the magnetic moment of the iron atom in the DFT case. The MCE was fitted on a set of configurations for which the magnitudes of magnetic moments of Fe and Cr are close to their values in the pure systems, and the error in the current case, where the moment is as small as 0.21 μ_B as predicted by DFT, may be substantially higher than the average accuracy of the MCE fit.

In a two-atom Fe cluster, the magnitude of moments at each Fe atom is 1.65 μ_B, i.e., it increases in comparison with

a single Fe atom case. The moments of the two Fe atoms are almost parallel to each other (the angle between them is 9°). With increasing cluster size, the magnitude of magnetic moment of Fe atoms increases, although more slowly than in DFT calculations (see Fig. 9). For a 5-atom cluster, the magnitude of moment on a Fe site is 1.73 μ_B. The angle between the average Fe moment in a cluster and the moment of Cr atoms in the matrix does not exhibit any systematic trend with increasing Fe cluster size, still most of the moments of iron atoms are close to being orthogonal to the neighboring Cr moments (see Table III). Also, starting from the smallest clusters, magnetic moments of Fe atoms do not stay in a single plane, but form three-dimensional structures, as it was in the case of Cr clusters in Fe with noncollinear magnetism (see, e.g., Fig. 16). Noncollinear configurations are always more stable than configurations calculated with collinear constraint, with the energy gain being the largest for a 3-atom cluster (160 meV/atom). The relative stability of noncollinear magnetic structures in Fe clusters is in agreement with almost all the clusters studied in DFT calculations (Table IV).

For a 9-atom cubic Fe cluster, the average magnitude of Fe moments at the cluster-matrix interface is 1.79 μ_B. This value increases towards the bulk value with increasing cluster size, reaching 2.13 μ_B for the largest studied 1241-atomic cubic Fe cluster. Similar behavior is observed for the octahedral iron clusters, where the average magnetic moment on Fe atoms increases from 1.76 μ_B for the 6-atom to 2.12 μ_B for the 1469-atom cluster.

The formation energy of all the Fe clusters is shown in Fig. 17. Single Fe atom has very high energy of over 400 meV, and with increasing cluster size the formation energy decreases, which means that the binding energy of iron atoms in clusters is positive (this is consistent with the DFT data) and is in agreement with the phase separation tendency characterizing the Fe-rich side of the Fe-Cr phase diagram. For large clusters, the formation energy is mainly the energy of Fe/Cr interfaces, as in the case of Cr clusters in Fe. As a result, the formation energies of Fe and Cr large clusters are almost the same because the interface areas are equal.

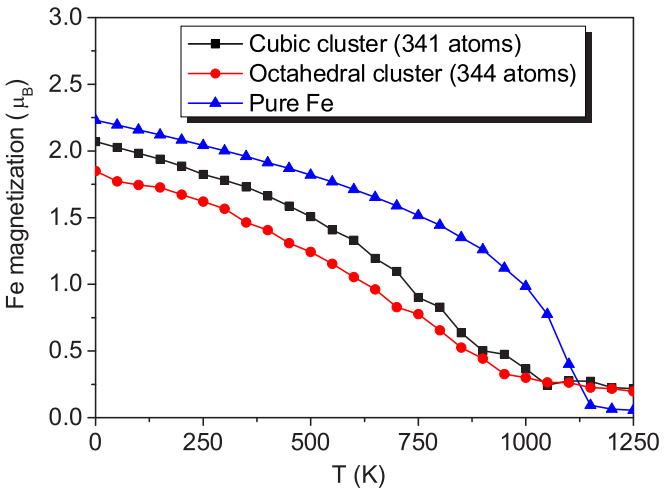

FIG. 23. (Color online) Temperature dependence of magnetization of cubic (341 atoms) and octahedral (344 atoms) Fe clusters, and magnetization of pure iron.

Similarly to the Cr-clusters case, for Fe clusters of more than 100 atoms, cubic clusters have lower formation energy than the octahedral clusters.

To study the temperature effects, we computed the magnetization of cubic and octahedral clusters as a function of temperature, and compared results with magnetization of pure Fe (Fig. 23). At low temperatures, noncollinearity results in decreasing magnetization, which is more pronounced for the octahedral clusters. At higher temperatures, magnetization of clusters decreases somewhat more rapidly than in pure Fe, which can be explained by disordering of Cr moments above the Néel temperature. Overall, we find weaker temperature variation of magnetization of Fe clusters compared to that of Cr clusters in iron. This can be explained by strong Fe-Fe magnetic interaction and relatively weak influence of Cr surrounding.

V. CONCLUSIONS

First-principles DFT and MCE Monte Carlo studies were carried out to find the lowest-energy magnetic configurations and explore finite-temperature magnetic properties of Cr clusters in FM bcc-iron and Fe clusters in AF bcc-Cr. In particular, we studied very small clusters, and clusters with (100) and/or (110) interfaces.

We showed, by means of noncollinear DFT calculations, that magnetic frustration caused by the competing Fe-Fe, Fe-Cr, and Cr-Cr magnetic-coupling tendencies determines the low-energy magnetic configurations of the clusters, inducing either small local magnetic moments or noncollinear structures, which partially release magnetic frustration. Small local atomic moments are often found in collinear ground states of Cr clusters in Fe. Noncollinear configurations are unstable for most of the studied Cr clusters, except for the clusters where interfacial Cr atoms dominate the structure, with either four or six Cr nearest neighbors, in which case noncollinear states are found as metastable local minima. A particularly interesting feature is the nonzero cluster magnetization caused by the dominance of Fe-Cr over Cr-Cr AF coupling in small and medium-size Cr clusters.

As opposed to the case of Cr clusters in Fe, noncollinear configurations commonly occur in Fe clusters, where they form as a way of relaxing magnetic frustration. In particular, noncollinear ground states are observed if the cluster size is sufficiently small ($N_{\mathrm{Fe}} \leqslant 5$) so that Fe-Cr AF coupling competes with, or even dominates over, Fe-Fe FM interactions. For larger clusters, all the Fe local moments remain parallel to each other. The energies of various collinear and noncollinear are generally not very dissimilar.

MCE simulations broadly agree with the DFT analysis, especially for the low-energy magnetic structures, and enable extending DFT results to much larger clusters and finite-temperature effects.

We found that the smallest Cr clusters in Fe matrix have collinear magnetic structure. Noncollinearity begins to appear at cluster sizes of at least 13 Cr atoms, and for smaller clusters deviations from collinearity are smaller than for larger ones. Energy gain from adopting a noncollinear ground state compared to the collinear state is smaller for cubic clusters than for octahedral clusters. The strongest deviation from

collinearity is observed for the interfacial atoms with four or five nearest Cr neighbors, with atoms having fewer nearest Cr neighbors being almost collinear to the iron matrix. The ferromagnetically ordered Fe matrix induces nonzero total magnetic moment in chromium clusters, which can be as high as 1 μ_B per atom in the limit of small cluster size.

The temperature dependence of magnetic properties of Cr clusters is strongly influenced by the Fe matrix. Strong Fe-Cr interaction results in the total magnetization of clusters remaining nonzero even at fairly high temperatures, close to the Curie temperature of pure Fe for larger clusters. Cr-Cr correlations also persist until higher temperatures due to magnetic coupling of interfacial Cr atoms with the Fe matrix. Interesting behavior of magnetic correlations is observed for the octahedral clusters, where they change sign from antiferromagnetic to ferromagnetic with increasing temperature. The reason for such change is the relatively large number of nearest-neighbor bonds between the interfacial Cr atoms with moments antiparallel to the Fe matrix and thus parallel to each other, especially at elevated temperatures. The temperature dependence of magnetization is simulated for various cluster sizes and assessed against experimental data. A possible link between the sharp drop of magnetization at elevated temperature, and the change of nanostructure of Fe-Cr alloy, proposed on the basis of experimental data, is confirmed by our simulations.

For small Fe clusters in Cr matrix, MCE results show that the formation of noncollinear magnetic structures is the most efficient way of relaxing magnetic frustration, in agreement with DFT findings. Temperature dependence of the total cluster magnetization is not as strong in comparison with the case of Cr clusters in iron.

Finally, this study shows the significance of using noncollinear magnetic approximations since noncollinear configurations of Fe and Cr clusters have energies lower than, or close to, the energies of collinear states, and thus likely occur even at relatively low temperatures. This is also to be expected in any alloys composed of elements exhibiting tendencies towards FM and AF magnetic ordering.

ACKNOWLEDGMENTS

This work was part-funded by the EuroFusion Consortium, and has received funding from Euratom research and training programme 2014–2018 under Grant Agreement No. 633053, and funding from the RCUK Energy Programme (Grant No. EP/I501045). The views and opinions expressed herein do not necessarily reflect those of the European Commission. All the DFT calculations were performed using resources of IFERC-CSC Helios supercomputer (Japan) within the project SISteel, and GENCI project (Grants No. x2014096020 and No. x2015096020). This work was also part-funded by the United Kingdom Engineering and Physical Sciences Research Council via a programme Grant No. EP/G050031. The authors would also like to acknowledge support of this collaboration from the French Embassy in the U. K.

[1] R. Klueh and A. Nelson, J. Nucl. Mater. **371**, 37 (2007).
[2] S. J. Zinkle and J. T. Busby, Mater. Today **12**, 12 (2009).
[3] S. L. Dudarev, J. L. Boutard, R. Lässer, M. J. Caturla, P. M. Derlet, M. Fivel, C.-C. Fu, M. Y. Lavrentiev, L. Malerba, M. Mrovec *et al.*, J. Nucl. Mater. **386–388**, 1 (2009).
[4] C. D. Hardie, C. A. Williams, S. Xu, and S. G. Roberts, J. Nucl. Mater. **439**, 33 (2013); M. Bachhav, G. R. Odette, and E. A. Marquis, Scr. Mater. **74**, 48 (2014).
[5] G. J. Ackland, Phys. Rev. Lett. **97**, 015502 (2006).
[6] T. P. C. Klaver, R. Drautz, and M. W. Finnis, Phys. Rev. B **74**, 094435 (2006).
[7] D. Nguyen-Manh, M. Y. Lavrentiev, and S. L. Dudarev, J. Comput.-Aided Mater. Des. **14**, 159 (2007).
[8] D. Nguyen-Manh, M. Y. Lavrentiev, and S. L. Dudarev, C. R. Physique **9**, 379 (2008).
[9] O. Senninger, E. Martinez, F. Soisson, M. Nastar, and Y. Brechet, Acta Mater. **73**, 9 (2014).
[10] A. V. Ruban, P. A. Korzhavyi, and B. Johansson, Phys. Rev. B **77**, 094436 (2008).
[11] M. Ropo, K. Kokko, E. Airiskallio, M. P. J. Punkkinen, S. Hogmark, J. Kollar, B. Johansson, and L. Vitos, J. Phys.: Condens. Matter **23**, 265004 (2011).
[12] P. A. Korzhavyi, A. V. Ruban, J. Odqvist, J. O. Nilsson, and B. Johansson, Phys. Rev. B **79**, 054202 (2009).
[13] A. Kiejna and E. Wachowicz, Phys. Rev. B **78**, 113403 (2008).
[14] P. Olsson, C. Domain, and J. Wallenius, Phys. Rev. B **75**, 014110 (2007).
[15] E. Martinez, O. Senninger, C.-C. Fu, and F. Soisson, Phys. Rev. B **86**, 224109 (2012).
[16] R. Soulairol, C.-C. Fu, and C. Barreteau, Phys. Rev. B **83**, 214103 (2011).
[17] H. Wen, P.-W. Ma, and C. H. Woo, J. Nucl. Mater. **440**, 428 (2013).
[18] H. Yamamoto, Jpn. J. Appl. Phys. **3**, 745 (1964).
[19] M. Y. Lavrentiev, D. Nguyen-Manh, and S. Dudarev, Solid State Phenom. **172–174**, 1002 (2011).
[20] R. Soulairol, C.-C. Fu, and C. Barreteau, J. Phys.: Condens. Matter **22**, 295502 (2010).
[21] A. Bergman, L. Nordström, A. Burlamaqui Klautau, S. Frota-Pessôa, and O. Eriksson, Phys. Rev. B **75**, 224425 (2007).
[22] V. S. Stepanyuk, W. Hergert, P. Rennert, K. Kokko, A. F. Tatarchenko, and K. Wildberger, Phys. Rev. B **57**, 15585 (1998).
[23] R. N. Igarashi, A. B. Klautau, R. B. Muniz, B. Sanyal, and H. M. Petrilli, Phys. Rev. B **85**, 014436 (2012).
[24] R. Robles and L. Nordstrom, Phys. Rev. B **74**, 094403 (2006).
[25] D. Nguyen-Manh and S. L. Dudarev, Phys. Rev. B **80**, 104440 (2009).
[26] R. C. Longo, A. Vega, S. Bouarab, J. Ferrer, M. M. G. Alemany, and L. J. Gallego, Phys. Rev. B **77**, 212406 (2008).
[27] M. Levesque, E. Martinez, C.-C. Fu, M. Nastar, and F. Soisson, Phys. Rev. B **84**, 184205 (2011).

[28] M. Y. Lavrentiev, R. Soulairol, C.-C. Fu, D. Nguyen-Manh, and S. L. Dudarev, Phys. Rev. B **84**, 144203 (2011).
[29] H. Fritzsche, S. Bonn, J. Hauschild, J. Klenke, K. Prokes, and G. J. McIntyre, Phys. Rev. B **65**, 144408 (2002).
[30] M. Y. Lavrentiev, D. Nguyen-Manh, and S. L. Dudarev, Phys. Rev. B **81**, 184202 (2010).
[31] M. Y. Lavrentiev, S. Dudarev, and D. Nguyen-Manh, J. Appl. Phys. **109**, 07E123 (2011).
[32] M. Y. Lavrentiev, K. Mergia, M. Gjoka, D. Nguyen-Manh, G. Apostolopoulos, and S. L. Dudarev, J. Phys.: Condens. Matter **24**, 326001 (2012).
[33] M. Y. Lavrentiev, J. S. Wróbel, D. Nguyen-Manh, and S. Dudarev, Phys. Chem. Chem. Phys. **16**, 16049 (2014).
[34] J. Soler, E. Artacho, J. Gale, A. Garcia, J. Junquera, P. Ordejón, and D. Sanchez-Portal, J. Phys.: Condens. Matter **14**, 2745 (2002).
[35] L. M. Sandratskii, Adv. Phys. **47**, 91 (1998).
[36] V. García-Suárez, C. Newman, C. Lambert, J. Pruneda, and J. Ferrer, J. Phys.: Condens. Matter **16**, 5453 (2004).
[37] J. P. Perdew, K. Burke, and M. Ernzerhof, Phys. Rev. Lett. **77**, 3865 (1996).
[38] R. Soulairol, C.-C. Fu, and C. Barreteau, Phys. Rev. B **84**, 155402 (2011).
[39] J. Sanchez, F. Ducastelle, and D. Gratias, J. Nucl. Mater. **128**, 334 (1984).
[40] M. Y. Lavrentiev, R. Drautz, D. Nguyen-Manh, T. P. C. Klaver, and S. L. Dudarev, Phys. Rev. B **75**, 014208 (2007).
[41] P. M. Derlet, Phys. Rev. B **85**, 174431 (2012).
[42] S. M. Dubiel, C. Sauer, and W. Zinn, Phys. Rev. B **30**, 6285 (1984).
[43] P. Alvarado, J. Dorantes-Dávila, and G. M. Pastor, Phys. Rev. B **58**, 12216 (1998).
[44] T. Jourdan, F. Soisson, E. Couet, and A. Barbu, Acta Mater. **58**, 3400 (2010).